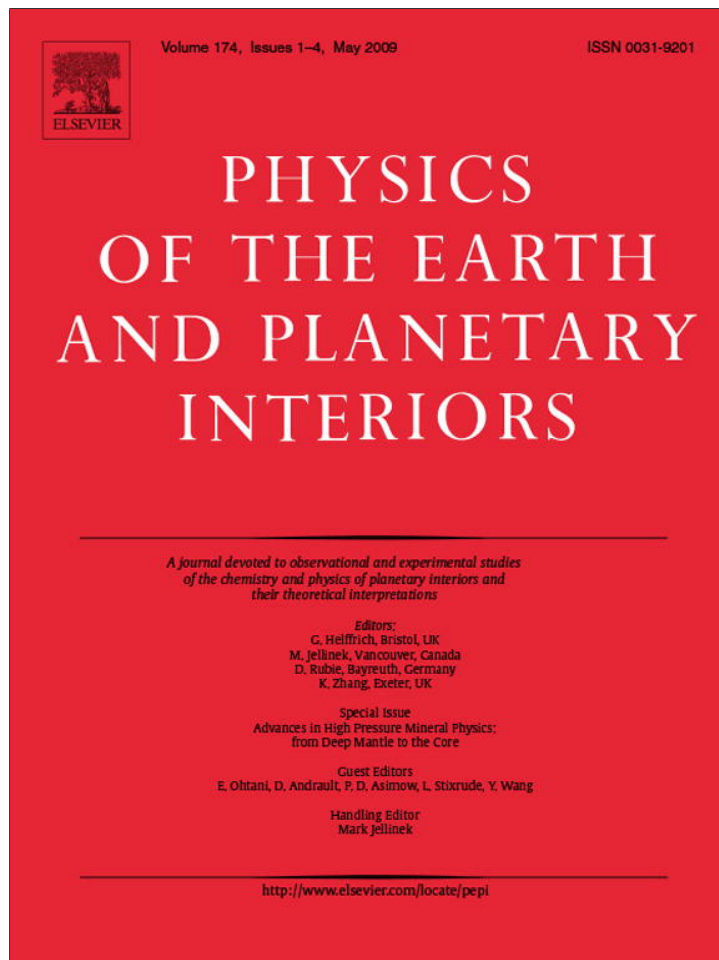


Provided for non-commercial research and education use.  
Not for reproduction, distribution or commercial use.



This article appeared in a journal published by Elsevier. The attached copy is furnished to the author for internal non-commercial research and education use, including for instruction at the authors institution and sharing with colleagues.

Other uses, including reproduction and distribution, or selling or licensing copies, or posting to personal, institutional or third party websites are prohibited.

In most cases authors are permitted to post their version of the article (e.g. in Word or Tex form) to their personal website or institutional repository. Authors requiring further information regarding Elsevier's archiving and manuscript policies are encouraged to visit:

<http://www.elsevier.com/copyright>



Contents lists available at ScienceDirect

## Physics of the Earth and Planetary Interiors

journal homepage: [www.elsevier.com/locate/pepi](http://www.elsevier.com/locate/pepi)Ab initio predictions of potassium partitioning between Fe and Al-bearing MgSiO<sub>3</sub> perovskite and post-perovskiteKanani K.M. Lee<sup>a,b,\*</sup>, Gerd Steinle-Neumann<sup>b</sup>, Sofia Akber-Knutson<sup>c</sup><sup>a</sup> Department of Physics, New Mexico State University, Las Cruces, NM 88003-8001, United States<sup>b</sup> Bayerisches Geoinstitut, Universität Bayreuth, D-95540 Bayreuth, Germany<sup>c</sup> Scripps Institution of Oceanography, University of California, San Diego, La Jolla, CA 92093, United States

## ARTICLE INFO

## Article history:

Received 29 September 2007

Received in revised form 9 July 2008

Accepted 1 September 2008

## Keywords:

Magnesium silicate perovskite

Post-perovskite

Lower mantle

High-pressure

Partitioning

Potassium

## ABSTRACT

Ab initio quantum mechanical computations suggest that potassium (K) preferentially partitions into MgSiO<sub>3</sub> perovskite (pv) over post-perovskite (ppv) under lower mantle conditions when charge coupled with trivalent cations of aluminum (Al<sup>3+</sup>) or iron (Fe<sup>3+</sup>). In an Al-bearing MgSiO<sub>3</sub>, the equilibrium constant  $K_D$  increases with pressure, leveling off at ~33 at ~100 GPa and 3000 K. For an Fe-bearing MgSiO<sub>3</sub>,  $K_D$  slowly increases with pressure reaching a value of ~8 at core-mantle boundary (CMB) pressures and 3000 K. Our results imply that a potassium-enriched lowermost mantle layer based on the stability of ppv is unlikely.

© 2008 Elsevier B.V. All rights reserved.

## 1. Introduction

Partitioning of long-lived radioactive isotopes (e.g., <sup>40</sup>K, <sup>235</sup>U, <sup>238</sup>U and <sup>232</sup>Th) in the Earth's interior is important to the thermal evolution of the Earth as radioactive decay provides an important source of energy for mantle dynamics. As a consequence, enriched (or depleted) reservoirs in the mantle influence the energy balance in geodynamics (Buffett, 2002; Labrosse and Jaupart, 2007). The recently discovered transition in MgSiO<sub>3</sub> from perovskite (pv) to post-perovskite (ppv) in the lowermost mantle causes a density increase by ~1–2% between the Mg-endmembers (Murakami et al., 2004; Oganov and Ono, 2004; Shim et al., 2004; Tsuchiya et al., 2004). In addition, as iron preferentially partitions into ppv (Caracas and Cohen, 2005; Mao et al., 2004; Ono and Oganov, 2005), a negatively buoyant Fe-rich ppv layer could play an important role as a stagnant layer. The negative buoyancy of this dense layer is a common trait (2–5% more dense than surrounding mantle) of many proposed thermochemical pile models that accumulate below mantle upwellings (e.g., Davaille, 1999; Lassak et al., 2007).

Such a dense layer at the base of the mantle based on the ppv phase could potentially also provide for a global radiogenically

enriched or depleted zone. Therefore, the partitioning of potassium (K) among the phases of the lower mantle is of central importance to the geochemistry and geodynamics of the deep Earth.

In the crust and upper mantle a number of K-rich phases exist (e.g., feldspars, micas and amphiboles) (Harlow and Davies, 2004) and many experiments on high-pressure potassium-rich phases have been conducted to search for possible lower mantle hosts for K (Ferroir et al., 2006; Guignot and Andrault, 2004; Nishiyama et al., 2005; Sueda et al., 2004; Tutti et al., 2001; Wang and Takahashi, 2000). However, due to the small abundance of potassium, ~240 ppm by weight (McDonough and Sun, 1995), a K-rich phase in the mantle is unexpected (Perrillat et al., 2006; Wang and Takahashi, 1999). Instead, potassium should be incorporated into one (or more) of the three major solid solutions in the mantle: iron (Fe) and aluminum (Al)-bearing MgSiO<sub>3</sub> in the perovskite or post-perovskite structure, magnesiowüstite (Mg, Fe)O and calcium silicate perovskite CaSiO<sub>3</sub> (Irifune and Ringwood, 1987; Kesson et al., 1998; Lee et al., 2004; Murakami et al., 2005; O'Neill and Jeanloz, 1990). As potassium is monovalent, to replace a cation in one of the three major solid solutions requires coupling to trivalent cations. The most abundant trivalent cations M<sup>3+</sup> in the Earth are iron and aluminum, both of which we test in this study.

Where potassium resides in the lower mantle may determine where this potentially important internal heat source is located. The pv–ppv phase transition is the only phase transition known in the lower mantle and the ppv bearing D' layer could consequently provide a distinct global reservoir for heat-producing potassium.

\* Corresponding author at: Department of Geology & Geophysics, Kline Geology Laboratory, 210 Whitney Avenue, New Haven, CT 06511, United States. Tel.: +1 203 432 4354; fax: +1 203 432 3134.

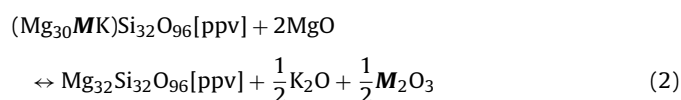
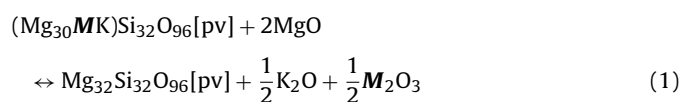
E-mail address: [kanani.lee@yale.edu](mailto:kanani.lee@yale.edu) (K.K.M. Lee).

We here explore this possibility by means of ab initio computations on the incorporation of K into MgSiO<sub>3</sub> pv and ppv at lower mantle pressures. In order to incorporate monovalent K into the pv or ppv structures, we choose to charge couple K<sup>+</sup> with Fe<sup>3+</sup> or Al<sup>3+</sup>, the most abundant trivalent cations in the lower mantle that are incorporated readily in MgSiO<sub>3</sub> pv (Frost and Langenhorst, 2002; Irifune, 1994; Zhang and Oganov, 2006a,b). In the computations we consider Fe and Al-bearing MgSiO<sub>3</sub> perovskites and their corresponding high-pressure polymorphs, Fe and Al-bearing MgSiO<sub>3</sub> post-perovskites.

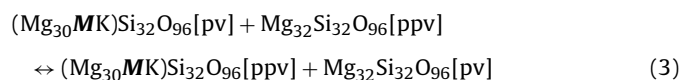
## 2. Methods

### 2.1. Supercell computations and energetics

To investigate K partitioning between pv and ppv we consider the following two reactions composed of oxides and 160-atom silicate supercells:



where **M** is Fe or Al. Combining reactions (1) and (2) yields a reaction with only pv and ppv terms:



where the oxide terms cancel. The energetics of this reaction will determine how K partitions between pv and ppv. In our computations for perovskite and post-perovskite, two Mg sites are allowed to have either an iron–potassium or an aluminum–potassium pair that replaces two Mg atoms at adjacent A (Mg)-sites, in order to locally charge balance the MgSiO<sub>3</sub> based solid solution in pv and ppv. The pv supercells are based on the orthorhombic *Pnma* structure and consist of 2 × 2 × 2 (160 atoms) orthorhombic cells. The ppv supercells are based on the orthorhombic *Cmcm* structure and consist of 4 × 1 × 2 (160 atoms) orthorhombic cells.

The electronic structure and energetics of the supercells used have been calculated by density functional theory (DFT)-based methods. DFT is exact except for the basic approximation for exchange and correlation that describes the many-body interactions of electrons in the system. We use the generalized gradient approximation (GGA) (Perdew et al., 1992) for all of our computations in order to assure compatibility of results as well as to compare with previous computations in the Mg–Fe–Al pv and ppv solid solutions (Akber-Knutson et al., 2005; Ono and Oganov, 2005; Stackhouse et al., 2007). We use the projector augmented wave method (PAW) (Kresse and Joubert, 1999) as implemented in the Vienna Ab initio Simulation Package (VASP) (Kresse and Furthmüller, 1996; Kresse and Hafner, 1993). As we consider high compressions, resulting in hybridization of low-lying electronic states, we chose potentials that treat the following electronic shells as valence: 3p, 3d and 4s for iron; 2p and 3s for magnesium; 3s, 3p and 4s for potassium; 3s and 3p for aluminum and silicon; and 2s and 2p for oxygen. These potentials have been used successfully by previous studies (Oganov and Ono, 2004; Ono and Oganov, 2005; Stackhouse et al., 2007). For the iron-bearing silicates, we perform spin-polarized computations.

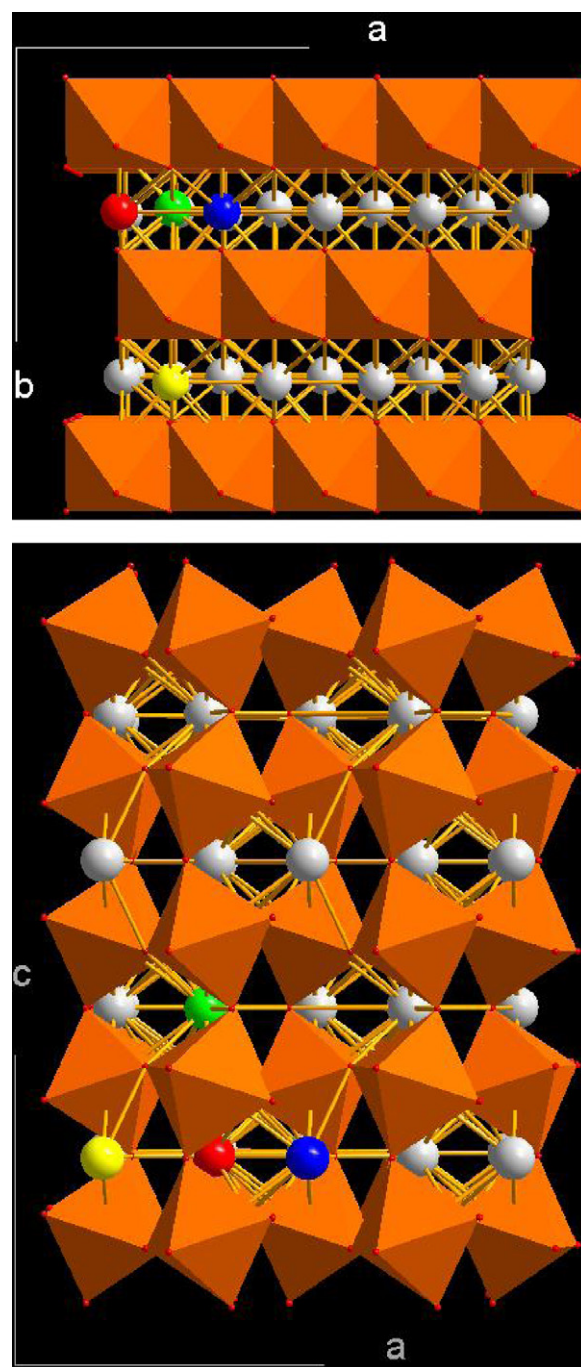


**Fig. 1.** (Top) Crystal structure of 160-atom supercell of (Mg<sub>30</sub>MK)Si<sub>32</sub>O<sub>96</sub> perovskite projected along *b*-axis. (Bottom) Crystal structure of 160-atom supercell of (Mg<sub>30</sub>MK)Si<sub>32</sub>O<sub>96</sub> post-perovskite projected along the *c*-axis. The red atom represents K. The three nearest-neighbor **M** atoms are represented by blue, green and yellow, with nn distances increasing. (For interpretation of the references to color in this figure legend, the reader is referred to the web version of the article.)

To establish the energetics of partitioning we must assure that absolute energies are well converged with respect to computational parameters. For the plane wave computations the critical computational parameters are the cut-off energy for the expansion of the charge density in a plane wave basis ( $E_{\text{cut}}$ ) and the number of reciprocal space vectors at which the Kohn–Sham equations are solved (*k*-points). For the 160 atom supercell convergence to within 3 meV/atom for absolute internal energies is achieved with  $E_{\text{cut}} = 1000$  eV and a single *k*-point ( $\Gamma$ ).

We have performed computations over a wide compression range from over-expanded to highly compressed volumes ( $V=120\text{--}180\text{ \AA}^3$ ). The energy–volume relations for the silicate supercells are fit with a Birch–Murnaghan equation of state (Birch, 1952).

## 2.2. Thermodynamics of potassium partitioning

In order to determine thermodynamic phase stability as well as partitioning, we compute the Gibbs free energy  $G=E+PV-TS$  for  $(\text{Mg}_{30}\text{MK})\text{Si}_{32}\text{O}_{96}$ , where  $E$  is the internal energy computed from static ab initio computations,  $P$  is pressure determined from the Birch–Murnaghan equation of state,  $V$  is volume,  $T$  is temperature and  $S$  is entropy, composed of two parts: the vibrational  $S_{\text{vib}}$  and configurational  $S_{\text{conf}}$ . Enthalpy  $H$  comprises the first two terms of the above expression for Gibbs free energy and is used in this study, since the computations are performed under static conditions at 0K. Additionally, as a previous study (Tsuchiya et al., 2005) found that the vibrational density of states and resulting thermodynamic properties of pv and ppv are nearly identical, we neglect the  $S_{\text{vib}}$  contribution to the entropy. We choose to keep the pairs of  $\text{M}^{3+}\text{--K}^+$  adjacent for local charge balance (Stackhouse et al., 2007). Since each pair could be placed in any pair of Mg sites in the supercell, there is a configurational entropy contribution to the free energy. However, as the number of Mg sites are the

same for both pv and ppv structures, the configurational entropy terms cancel for the reaction between  $(\text{Mg}_{30}\text{MK})\text{Si}_{32}\text{O}_{96}$  pv and ppv (reaction (3)).

The equilibrium constant of potassium ( $K_D$ ) between pv and ppv is defined by the thermodynamics relation below, where  $k_B$  is Boltzmann's constant and  $T$  is temperature. Using Henry's Law, we determine the equilibrium constant  $K_D$  in terms of a ratio of the mole concentrations of K in pv ( $x_{\text{K,pv}}$ ) and in ppv ( $x_{\text{K,ppv}}$ ) (Table 2):

$$K_D \equiv \exp\left(\frac{-\Delta G}{k_B T}\right) = \frac{(x_{\text{K,pv}})(1-x_{\text{K,ppv}})}{(x_{\text{K,ppv}})(1-x_{\text{K,pv}})} \quad (4)$$

where instead of  $\Delta G$  we use  $\Delta H$  assuming the entropy terms cancel, following the arguments above.

## 2.3. Nearest-neighbor configurations

To check the validity of using a single nearest-neighbor (nn) A–A site (i.e., nominally between the Mg sites) pair for the trivalent–monovalent substitution, we compute the internal energies for three different nn distances. The three nn pairs are nearly orthogonal to each other, along a, b and c axes from the reference K atom (Fig. 1). Their distances are 2.96 (2.45), 3.20 (3.28) and 4.06 (4.19) Å for  $\text{MgSiO}_3$  in the pv (ppv) structure respectively near CMB pressures (unit-cell volume of  $120\text{ \AA}^3$ ). For these three configurations the internal energies are within  $\sim 2$  meV/atom, within

**Table 1**

Birch–Murnaghan equation of state parameters for the pure Mg-endmember, Fe and Al-bearing perovskite and post-perovskite (Birch, 1952). Uncertainties (measure of goodness of Birch–Murnaghan fits) are given in parentheses. K concentration in the last column is in wt% ppm.  $V_0$  is the zero pressure unit-cell volume of pv or ppv (20 atoms),  $K_0$  is the bulk modulus at zero pressure, its pressure derivative  $K'_0$  and the minimum energy  $E_0$  per unit cell.

		$V_0$ ( $\text{\AA}^3$ )	$K_0$ (GPa)	$K'_0$	$E_0$ (eV)	K concentration (wt% ppm)
<b>Perovskite</b>						
$\text{Mg}_{32}\text{Si}_{32}\text{O}_{96}$	This study	167.49 (0.02)	231 (1)	3.94 (0.02)	–139.967 (0.002)	0
$(\text{Mg}_{30}\text{FeK})\text{Si}_{32}\text{O}_{96}$	This study	168.78 (0.02)	230 (1)	3.96 (0.02)	–139.699 (0.002)	$\sim 12,000$
$(\text{Mg}_{30}\text{AlK})\text{Si}_{32}\text{O}_{96}$	This study	168.45 (0.02)	230 (1)	3.96 (0.01)	–139.599 (0.002)	$\sim 12,100$
$\text{MgSiO}_3$	Theory, GGA (Akber-Knutson et al., 2005)	167	235	3.84		0
$(\text{Mg}_{0.9375}\text{Al}_{0.0625})(\text{Si}_{0.9375}\text{Al}_{0.0625})\text{O}_3$	Theory, GGA (Akber-Knutson et al., 2005)	167.44	232	3.86		0
$\text{MgSiO}_3$	Theory, GGA (Caracas and Cohen, 2005)	163.12	232	3.86		0
$(\text{Mg}_{0.5}\text{Fe}_{0.5})\text{SiO}_3$	Theory, GGA (Caracas and Cohen, 2005)	170.68	231	4.03		0
$\text{MgSiO}_3$	Experiment (Mao et al., 1991)	162.49 (0.07)	261 (4)	4 <sup>a</sup>		0
$(\text{Mg}_{0.9}\text{Fe}_{0.1})\text{SiO}_3$	Experiment (Mao et al., 1991)	162.79 (0.08)	261 (4)	4 <sup>a</sup>		0
$(\text{Mg}_{0.8}\text{Fe}_{0.2})\text{SiO}_3$	Experiment (Mao et al., 1991)	163.53 (0.10)	261 (4)	4 <sup>a</sup>		0
$\text{MgSiO}_3$	Experiment (Walter et al., 2004)	162.47	267.3 (6.9)	4 <sup>a</sup>		0
$\text{MgSiO}_3$ with 5 mol% $\text{AlO}_{1.5}$	Experiment (Walter et al., 2004)	162.95	268.9 (7.0)	4 <sup>a</sup>		0
<b>Post-perovskite</b>						
$\text{Mg}_{32}\text{Si}_{32}\text{O}_{96}$	This study	167.82 (0.04)	199 (1)	4.33 (0.03)	–139.085 (0.003)	0
$(\text{Mg}_{30}\text{FeK})\text{Si}_{32}\text{O}_{96}$	This study	169.45 (0.04)	195 (1)	4.38 (0.03)	–138.817 (0.003)	$\sim 12,000$
$(\text{Mg}_{30}\text{AlK})\text{Si}_{32}\text{O}_{96}$	This study	169.15 (0.06)	195 (1)	4.38 (0.04)	–138.654 (0.004)	$\sim 12,100$
$\text{MgSiO}_3$	Theory, GGA (Akber-Knutson et al., 2005)	167.32	204	4.18		0
$(\text{Mg}_{0.9375}\text{Al}_{0.0625})(\text{Si}_{0.9375}\text{Al}_{0.0625})\text{O}_3$	Theory, GGA (Akber-Knutson et al., 2005)	167.16	207	4.18		0
$\text{MgSiO}_3$	Theory, GGA (Caracas and Cohen, 2005)	163.2	203	4.19		0
$(\text{Mg}_{0.5}\text{Fe}_{0.5})\text{SiO}_3$	Theory, GGA (Caracas and Cohen, 2005)	170.96	206	4.23		0

<sup>a</sup>  $K'_0$  held constant.

the convergence limit of the computations. Configurations at larger neighbor distances are not expected to yield favorable energetics due to the requirement of local charge balance (Stackhouse et al., 2007; Zhang and Oganov, 2006b).

### 3. Results

#### 3.1. Birch–Murnaghan equations of state

The equations of state of the (Fe, K) and (Al, K)-bearing silicates are similar, and show a slight increase in the zero-pressure volume  $V_0$  relative to  $\text{MgSiO}_3$  pv and ppv, while the zero-pressure bulk modulus  $K_0$  and its pressure derivative  $K'_0$  is virtually unchanged (Table 1), similar to other doped  $\text{MgSiO}_3$  perovskites (Akber-Knutson et al., 2005; Caracas and Cohen, 2005; Walter et al., 2004) and post-perovskites (Akber-Knutson et al., 2005; Caracas and Cohen, 2005). We also determine the transition pressure at static conditions for pv to ppv for each composition

and find 97, 103 and 107 GPa for  $\text{MgSiO}_3$ ,  $(\text{Mg}_{30}\text{FeK})\text{Si}_{32}\text{O}_{96}$  and  $(\text{Mg}_{30}\text{AlK})\text{Si}_{32}\text{O}_{96}$ , respectively. This suggests that the addition of K charge coupled with Al or Fe stabilizes pv over ppv. As the addition of Fe into pv tends to decrease the pv–ppv transition pressure (Caracas and Cohen, 2005; Zhang and Oganov, 2006b) while the addition of Al tends to increase the pv–pp transition pressure (Akber-Knutson et al., 2005; Caracas and Cohen, 2005), K increases the transition pressure but less so in the Fe-bearing pv.

#### 3.2. Local structure around K, Fe and Al

We compare the pressure-dependent distances between the nearest-neighbor trivalent–monovalent pairs with those between nearest Mg–Mg pairs in the pure endmembers (Fig. 2a). For all volumes investigated, the K-bearing pv phases show shorter nearest-neighbor distances than the pure Mg endmember. The nearest-neighbor distance between magnesium atoms in the

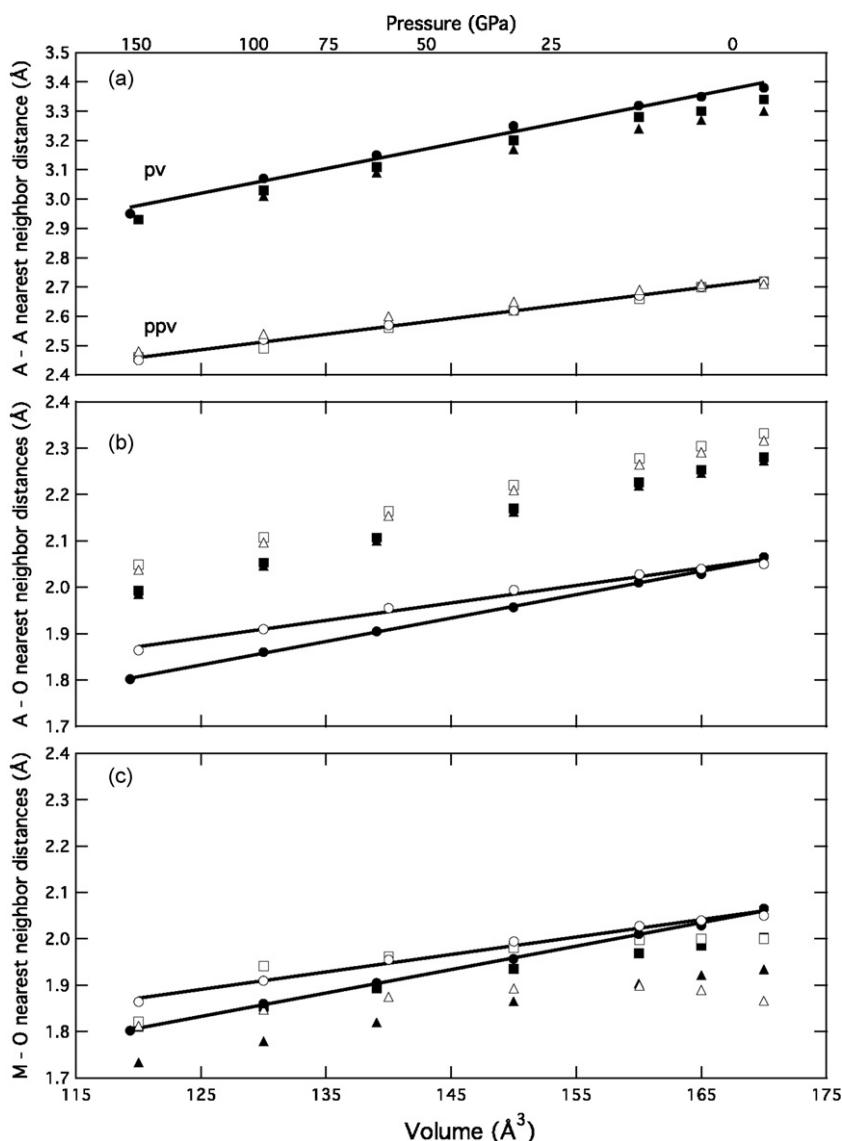


**Fig. 2.** (a) Nearest-neighbor distances of trivalent–monovalent pairs  $\text{Fe}^{3+}\text{--K}^+$  in  $(\text{Mg}_{30}\text{FeK})\text{Si}_{32}\text{O}_{96}$  (squares) and  $\text{Al}^{3+}\text{--K}^+$  in  $(\text{Mg}_{30}\text{AlK})\text{Si}_{32}\text{O}_{96}$  (triangles) in the pv (closed symbols) and ppv (open symbols) structures vs. volume compared to the Mg endmember (circles). Along the top axis, corresponding pressures for the Mg endmember pv are given. Lines represent the best linear fit to the Mg-endmembers. (b) Distances between K–O in  $(\text{Mg}_{30}\text{FeK})\text{Si}_{32}\text{O}_{96}$  (squares) and in  $(\text{Mg}_{30}\text{AlK})\text{Si}_{32}\text{O}_{96}$  (triangles) compared to Mg–O in the Mg endmember (circles). (c) Corresponding Fe–O (squares), Al–O (triangles) distances as well as Mg–O for the Mg endmember (circles) are plotted for comparison.

Mg-endmember ppv is nearly equal to the nearest-neighbor distances in K-bearing ppv. This suggests that there may be some geometric restriction in ppv to the Fe<sup>3+</sup>–K<sup>+</sup> or Al<sup>3+</sup>–K<sup>+</sup> pairs. The energetics support this observation as discussed below.

To compare the dodecahedral space potassium takes up in the pv or ppv structure, we show the nearest O neighbor, K–O distance in the (Fe, K) and (Al, K)-bearing silicates with that of the Mg–O distance of the Mg endmembers (Fig. 2b). As expected, we find that K takes up a larger space than the Mg.

This larger space is compensated by a reduced space used by the paired Fe<sup>3+</sup> or Al<sup>3+</sup> cation (Fig. 2c). Al in pv reduces the A-site considerably, and there is a parallel trend in Al–O distances to Mg–O under compression. Fe in pv has a slightly smaller Fe–O distance near ambient compression; at high compression it approaches that of Mg–O. This is approximately consistent with expected trends from ionic radii (Shannon and Prewitt, 1969). Al–O distances in ppv are considerably smaller than the equilibrium Mg–O distances, but begin to converge at high compression. At large volumes, far outside the stability range of the ppv phase, the Al–O distance decreases with increasing volume. The Fe–O distances, in contrast, stay approximately constant over a wide compression range (130–170 Å<sup>3</sup>) first with a larger distance than the Mg–O then a smaller distance. At the smallest volume considered (120 Å<sup>3</sup>, ~150 GPa) the Fe–O distance decreases significantly. This drop can be rationalized by the loss of magnetism in iron at 120 Å<sup>3</sup> (see below), which is essentially constant at the other volumes investigated (Fig. 2c).

### 3.3. Magnetization of Fe-bearing pv and ppv

The (Fe, K)-bearing phases remain in the high-spin state, with the magnetization decreasing from ~3.94 (3.87) μ<sub>B</sub> at 170 Å<sup>3</sup> to ~3.87 (3.90) μ<sub>B</sub> at 130 Å<sup>3</sup> in pv (ppv). For the Fe–K ppv, we find a sudden drop in the magnetization, from 3.90 to 2.47 μ<sub>B</sub>, between 130 and 120 Å<sup>3</sup> (corresponding to pressures of 93 and 145 GPa, respectively) while for pv the magnetic moment at 120 Å<sup>3</sup> (3.87 μ<sub>B</sub>) is consistent with the larger volumes. This high-spin to low-spin transition is reflected in a decreased space that the Fe<sup>3+</sup> takes up in the Fe–K ppv (Fig. 2c).

### 3.4. Reactions energetics and partitioning

We compute the difference in enthalpy ΔH in the equilibrium reaction (3) (Fig. 3, Table 2). At 0K, we find that at all mantle pressures, K prefers the pv over ppv structure for both the Fe and Al-bearing silicate, with Fe making ppv slightly more receptive to K than the Al-bearing counterpart. For the (Fe, K)-bearing reaction, we find the ΔH ~ 0.54 eV, in contrast with a ΔH ~ 0.89 eV for the (Al, K)-bearing reaction (Table 2). This suggests stronger K partitioning

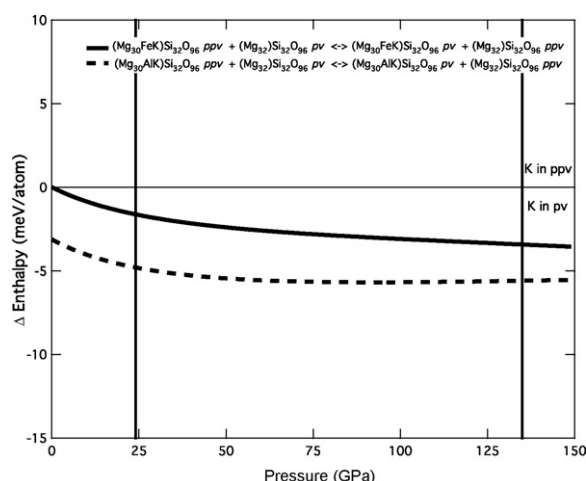


Fig. 3. ΔH per atom vs. pressure for reaction (3): (Mg<sub>30</sub>MK)Si<sub>32</sub>O<sub>96</sub>[ppv] + Mg<sub>32</sub>Si<sub>32</sub>O<sub>96</sub>[pv] ↔ (Mg<sub>30</sub>MK)Si<sub>32</sub>O<sub>96</sub>[pv] + Mg<sub>32</sub>Si<sub>32</sub>O<sub>96</sub>[ppv]. The solid curve corresponds to M = Fe and the dashed curve to M = Al. Negative ΔH values correspond to K preferring the pv structures, whereas positive ΔH values correspond to K favoring ppv structures. The two vertical lines indicate to the pressures of the upper–lower mantle boundary (~24 GPa) and the core–mantle boundary (~136 GPa).

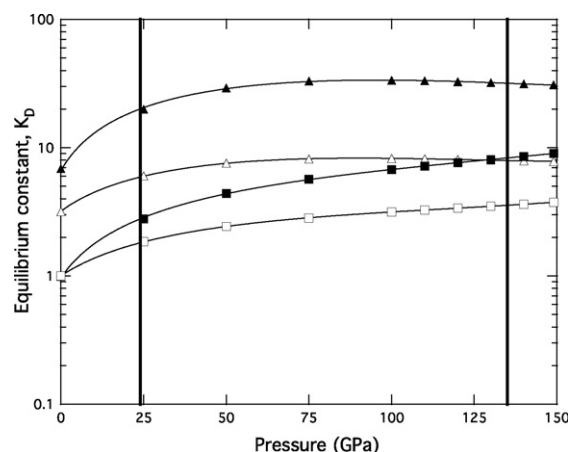


Fig. 4. Equilibrium constant,  $K_D$  vs. pressure between (Mg<sub>30</sub>FeK)Si<sub>32</sub>O<sub>96</sub> (squares) and between (Mg<sub>30</sub>AlK)Si<sub>32</sub>O<sub>96</sub> (triangles) pv and ppv computed at 3000 K (filled) and 5000 K (open), respectively. Thick vertical lines represent boundaries between the upper and lower mantle (~24 GPa) and the core and mantle (~136 GPa).

Table 2

Differences in enthalpy ΔH and equilibrium constant  $K_D$  of potassium between pv and ppv reaction (3) for (Mg<sub>30</sub>FeK)Si<sub>32</sub>O<sub>96</sub> and (Mg<sub>30</sub>AlK)Si<sub>32</sub>O<sub>96</sub>.  $K_D$  values of less than 1 indicate better K solubility in ppv than pv. Increasing the temperature decreases  $K_D$  for a given silicate composition (note:  $K_D = 1$  as  $T \rightarrow \infty$ ), thus allowing more K to partition into the ppv structure.

P (GPa)	ΔH (Fe, K) (eV)	$K_D$ (Mg <sub>30</sub> FeK)Si <sub>32</sub> O <sub>96</sub> at 3000 K	$K_D$ (Mg <sub>30</sub> FeK)Si <sub>32</sub> O <sub>96</sub> at 5000 K	ΔH (Al, K) (eV)	$K_D$ (Mg <sub>30</sub> AlK)Si <sub>32</sub> O <sub>96</sub> at 3000 K	$K_D$ (Mg <sub>30</sub> AlK)Si <sub>32</sub> O <sub>96</sub> at 5000 K
0	0.001	1.0	1.0	–0.498	6.9	3.2
25	–0.265	2.8	1.9	–0.774	19.9	6.0
50	–0.383	4.4	2.4	–0.872	29.2	7.6
75	–0.449	5.7	2.8	–0.904	33.0	8.2
100	–0.494	6.8	3.1	–0.908	33.5	8.2
110	–0.510	7.2	3.3	–0.906	33.2	8.2
120	–0.525	7.6	3.4	–0.902	32.7	8.1
130	–0.540	8.1	3.5	–0.897	32.1	8.0
150	–0.569	9.0	3.7	–0.887	30.9	7.8

in the Al-bearing pv than the Fe-bearing pv at a given temperature.

At high temperatures, the equilibrium constant  $K_D$  remains essentially flat over the pressures of the lower mantle (Table 2, Fig. 4). At 3000 K,  $K_D$  is  $\sim 33$  over lower mantle pressures for  $(\text{Mg}_{30}\text{AlK})\text{Si}_{32}\text{O}_{96}$  but decreases to  $<10$  at 5000 K. The equilibrium constant  $K_D$  for  $(\text{Mg}_{30}\text{FeK})\text{Si}_{32}\text{O}_{96}$  slowly increases at both 3000 and 5000 K to  $\sim 8$  and  $\sim 3$  at lowermost mantle pressures, respectively.

#### 4. Discussion and conclusions

We find that although potassium is a large atom at ambient conditions, when charge-coupled with trivalent Fe or Al and used to replace two adjacent Mg atoms, the combination can be accommodated into the pv structure (Fig. 2). This is similar to partitioning studies by Andraut (2003) which found that the pv structure can hold a variety of trivalent cations. Andraut concluded, however, that on the basis of relatively low partitioning of  $\text{Na}^+$  into pv that  $\text{K}^+$  would also be low due to its large size. We find otherwise, when  $\text{K}^+$  is coupled with trivalent Fe and Al.

Experiments on natural samples give diverging results on the host of alkali metal-bearing phases of the lower mantle. Multianvil experiments on a pyrolitic sample at uppermost lower mantle pressures found that Na prefers magnesiowüstite (mw) over pv (Tronnes and Frost, 2002). High-pressure, high-temperature diamond-anvil cell quench experiments on a pyrolite composition (Kesson et al., 1998) show that potassium prefers  $\text{CaSiO}_3$  (cpv) at 70 and 135 GPa. Sodium, on the other hand, is also detected in pv (trace amounts) and mw at mid-mantle pressures, but only in mw and cpv at 135 GPa (Kesson et al., 1998). On the other hand, Murakami et al. (2005) find that Na goes into all three lower mantle phases: pv, mw and cpv, although preferably into mw. Upon the transition of the pv to ppv, Na is continued to be measured in ppv. With the diversity of results from experiments, computations can shed additional light on the partitioning of K between lower mantle phases. Our results provide a first step in this process and computations on partitioning of potassium among all mantle phases will supplement the current results. Additionally, how K partitions between the mantle phases and the underlying iron-rich core will give additional information on heat distribution throughout the deep Earth.

The coupling of potassium with that of trivalent Fe or Al may also be enhanced due to the expected high amount of ferric iron available in the lower mantle as suggested by high-pressure experiments (Frost and Langenhorst, 2002; Frost et al., 2004) and measurements on samples from deep in the Earth (McCammon, 2005).

Our results imply that potassium is preferentially partitioned into pv in the Earth's mantle, which makes an enriched lowermost mantle layer based on the stability of ppv unlikely. Even if a dense layer of Fe-rich ppv could be maintained at depth due to preferential partitioning of Fe into ppv (Caracas and Cohen, 2005; Mao et al., 2004; Ono and Oganov, 2005) it would not be enriched in potassium.

#### Acknowledgements

K.K.M.L. would like to thank the Alexander von Humboldt Foundation and the Bayerisches Geoinstitut for the opportunity to conduct these computations. The collaboration has been supported by the Bavaria California Technology Center (BaCaTeC). Additionally, we would like to thank two anonymous reviewers for their constructive comments.

#### References

- Akber-Knutson, S., Steinle-Neumann, G., Asimow, P.D., 2005. Effect of Al on the sharpness of the  $\text{MgSiO}_3$  perovskite to post-perovskite phase transition. *Geophysical Research Letters* 32, L14303, doi:10.1029/2005GL023192.
- Andraut, D., 2003. Cationic substitution in  $\text{MgSiO}_3$  perovskite. *Physics of Earth and Planetary Interiors* 136, 67–78.
- Birch, F., 1952. Elasticity and constitution of the Earth's interior. *Journal of Geophysical Research* 57, 227–286.
- Buffett, B.A., 2002. Estimates of heat flow in the deep mantle based on the power requirements for the geodynamo. *Geophysical Research Letters* 29 (12), 1566.
- Caracas, R., Cohen, R.E., 2005. Effect of chemistry on the stability and elasticity of the perovskite and post-perovskite phases in the  $\text{MgSiO}_3$ – $\text{FeSiO}_3$ – $\text{Al}_2\text{O}_3$  system and implications for the lowermost mantle. *Geophysical Research Letters* 32, L16310, doi:10.1029/2005GL023164.
- Davaille, A., 1999. Simultaneous generation of hotspots and superwells by convection in a heterogeneous planetary mantle. *Nature* 402, 756–760.
- Ferroir, T., et al., 2006. Equation of state and phase transition in  $\text{KAlSi}_3\text{O}_8$  hollandite at high pressure. *American Mineralogist* 91, 327–332.
- Frost, D.J., Langenhorst, F., 2002. The effect of  $\text{Al}_2\text{O}_3$  on Fe–Mg partitioning between magnesiowüstite and magnesium silicate perovskite. *Earth and Planetary Science Letters* 199, 227–241.
- Frost, D.J., et al., 2004. Experimental evidence for the existence of iron-rich metal in the Earth's lower mantle. *Nature* 428, 409–412.
- Guignot, N., Andraut, D., 2004. Equations of state of Na–K–Al host phases and implications for MORB density in the lower mantle. *Physics of Earth and Planetary Interiors* 143/144, 107–128.
- Harlow, G.E., Davies, R., 2004. Status report on stability of K-rich phases at mantle conditions. *Lithos* 77, 647–653.
- Irfune, T., 1994. Absence of an aluminous phase in the upper part of the Earth's lower mantle. *Nature* 379, 131–133.
- Irfune, T., Ringwood, A.E., 1987. Phase transitions in primitive MORB and pyrolite compositions to 25 GPa and some geophysical implications. In: Manghnani, M.H., Syono, Y. (Eds.), *High-pressure Research in Mineral Physics*. American Geophysical Union, Washington, DC, pp. 231–242.
- Kesson, S.E., Fitzgerald, J.D., Shelley, J.M., 1998. Mineralogy and dynamics of a pyrolite lower mantle. *Nature* 393, 252–255.
- Kresse, G., Furthmüller, J., 1996. Efficient iterative schemes for ab initio total-energy calculations using a plane-wave basis set. *Physics Review B* 54 (16), 11169–11186.
- Kresse, G., Hafner, J., 1993. Ab initio molecular dynamics for liquid metals. *Physics Review B* 47 (1), 558–561.
- Kresse, G., Joubert, D., 1999. From ultrasoft pseudopotentials to the projector augmented-wave method. *Physics Review B* 59 (3), 1758–1775.
- Labrosse, S., Jaupart, C., 2007. Thermal evolution of the Earth: Secular changes and fluctuations of plate characteristics. *Earth and Planetary Science Letters* 260, 465–481.
- Lassak, T., McNamara, A.K., Zhong, S., 2007. Influence of thermochemical piles on topography at Earth's core–mantle boundary. *Earth and Planetary Science Letters* 261, 443–455.
- Lee, K.K.M., et al., 2004. Equations of state of high-pressure phases of a natural peridotite and implications for the Earth's lower mantle. *Earth and Planetary Science Letters* 223, 381–393.
- Mao, H.K., et al., 1991. Effect of pressure, temperature, and composition on lattice parameters and density of (Fe, Mg) $\text{SiO}_3$ –perovskites to 30 GPa. *Journal of Geophysical Research* 96 (B5), 8069–8079.
- Mao, W.L., et al., 2004. Ferromagnesian postperovskite silicates in the D'' layer of the Earth. *Proceedings of the National Academy of Sciences* 101 (45), 15867–15869.
- McCammon, C.A., 2005. Mantle oxidation state and oxygen fugacity: constraints on Earth accretion and early differentiation. In: van der Hilst, R.D., Bass, J., Matas, J., Trampert, J. (Eds.), *Structure, Composition and Evolution of Earth's Mantle*. American Geophysical Union, Washington, DC.
- McDonough, W.F., Sun, S.-S., 1995. The composition of the Earth. *Chemical Geology* 120, 223–253.
- Murakami, M., Hirose, K., Kawamura, K., Sata, N., Ohishi, Y., 2004. Post-perovskite phase transition in  $\text{MgSiO}_3$ . *Science* 304, 855–858.
- Murakami, M., Hirose, K., Sata, N., Ohishi, Y., 2005. Post-perovskite phase transition and mineral chemistry in the pyrolitic lowermost mantle. *Geophysical Research Letters* 32, L03304, doi:10.1029/2004GL021956.
- Nishiyama, N., et al., 2005. Stability and P–V–T equation of state of  $\text{KAlSi}_3\text{O}_8$ –hollandite determined by in situ x-ray observations and implications for dynamics of subducted continental crust material. *Physics and Chemistry of Minerals* 32, 627–637.
- O'Neill, B., Jeanloz, R., 1990. Experimental petrology of the lower mantle: a natural peridotite taken to 54 GPa. *Geophysical Research Letters* 17 (10), 1477–1480.
- Oganov, A.R., Ono, S., 2004. Theoretical and experimental evidence for a post-perovskite phase of  $\text{MgSiO}_3$  in Earth's D'' layer. *Nature* 430, 445–448.
- Ono, S., Oganov, A.R., 2005. In situ observations of phase transition between perovskite and  $\text{CaIrO}_3$ -type phase in  $\text{MgSiO}_3$  and pyrolitic mantle composition. *Earth and Planetary Science Letters* 236 (2005), 914–932.
- Perdew, J.P., et al., 1992. Atoms, molecules, solids, and surfaces: Applications of the generalized gradient approximation for exchange and correlation. *Physics Review B* 46 (11), 6671–6687.
- Perrillat, J.P., et al., 2006. Phase transformations of subducted basaltic crust in the uppermost lower mantle. *Physics of Earth and Planetary Interiors* 157, 139–149.

- Shannon, R.D., Prewitt, C.T., 1969. Effective ionic radii in oxides and fluorides. *Acta Crystallographica B* 25, 925–946.
- Shim, S.H., Duffy, T.S., Jeanloz, R., Shen, G., 2004. Stability and crystal structure of  $\text{MgSiO}_3$  perovskite to the core-mantle boundary. *Geophysical Research Letters* 31, L1063.
- Stackhouse, S., Brodholt, J., Price, G.D., 2007. Electronic spin transitions in iron-bearing  $\text{MgSiO}_3$  perovskite. *Earth and Planetary Science Letters* 253, 282–290.
- Sueda, Y. et al., 2004. A new high-pressure form of  $\text{KAlSi}_3\text{O}_8$  under lower mantle conditions. 31 (L23612). *Geophysical Research Letters*, doi:10.1029/2004GL021156.
- Tronnes, R.G., Frost, D.J., 2002. Peridotite melting and mineral-melt partitioning of major and minor elements at 22–24.5 GPa. *Earth and Planetary Science Letters* 197, 117–131.
- Tsuchiya, J., Tsuchiya, T., Wentzcovitch, R.M., 2005. Vibrational and thermodynamical properties of  $\text{MgSiO}_3$  postperovskite. *Journal of Geophysical Research* 110., B02204, doi:10.1029/2004JB003409.
- Tsuchiya, T., Tsuchiya, J., Umemoto, K., Wentzcovitch, R.M., 2004. Phase transition in  $\text{MgSiO}_3$  perovskite in the Earth's mantle. *Earth and Planetary Science Letters* 224, 241–248.
- Tutti, F., Dubrovinsky, L.S., Saxena, S.K., Carlson, S., 2001. Stability of  $\text{KAlSi}_3\text{O}_8$  Hollandite-type structure in the Earth's lower mantle conditions. *Geophysical Research Letters* 28 (14), 2735–2738.
- Walter, M.J., et al., 2004. Phase relations and equation-of-state of aluminous Mg-silicate perovskite and implications for Earth's lower mantle. *Earth and Planetary Science Letters* 222, 501–516.
- Wang, W., Takahashi, E., 1999. Subsolidus and melting experiments of a K-rich basaltic composition to 27 GPa: Implication for the behavior of potassium in the mantle. *American Mineralogist* 84, 357–361.
- Wang, W., Takahashi, E., 2000. Subsolidus and melting experiments of K-doped peridotite KLB-1 to 27 GPa: Its geophysical and geochemical implications. *Journal of Geophysical Research* 105 (B2), 2855–2868.
- Zhang, F., Oganov, A.R., 2006a. Mechanisms of  $\text{Al}^{3+}$  incorporation in  $\text{MgSiO}_3$  post-perovskite at high pressures. *Earth and Planetary Science Letters* 248, 69–76.
- Zhang, F., Oganov, A.R., 2006b. Valence state and spin transitions of iron in Earth's mantle silicates. *Earth and Planetary Science Letters* 249, 436–443.